Assessing the Feasibility of Markerless Close Range Photogrammetry in Industrial Inspection: A Foundational Study

Ines Prieto[1], Pablo Puerto[1], Ibai Leizea[1], Imanol Herrera[1]

[1] IDEKO, Basque Research and Technology Alliance (BRTA), 20870 Elgoibar, Spain
iprieto@ideko.es

Technical Commission II

Keywords: Large-volume metrology; Markerless photogrammetry; Accuracy measurement; 3D Reconstruction.

Abstract

As large-volume metrology gains significance in industrial applications, ensuring high-accuracy measurements (±0.1 mm) with cost-effective and user-friendly technologies becomes increasingly challenging. This study evaluates the performance of Markerless Photogrammetry (MP) against industry standards such as Coordinate Measuring Machines (CMM), Laser Trackers (LT), and Marker-based Photogrammetry (MbP) to identify the potential of MP in addressing industrial challenges. While CMM and LT offer high accuracy, their applicability is limited by the size of large workpieces and cost. MbP offers high work ranges, flexibility and ease of use, but it is restricted to sparse measurements and lacks the accuracy of traditional methods. Despite its lower accuracy, the results indicate that MP may present a viable solution for cases where cost-effectiveness and ease of use are crucial with the drawback of high computational cost.

1. Introduction

The growing importance of large-volume (above $3m^3$) metrology in industrial settings brings with it specific challenges, such as ensuring high accuracy measurements (±0.1 mm) with cost-efficient, easy to use technologies. This presents a considerable obstacle for sectors such as aerospace, heavy equipment manufacturing, energy, and general engineering (Savio et al., 2007).

Traditionally, smaller parts are often measured with Coordinate Measuring Machines (CMMs) for high accuracy instead of Laser trackers (LTs) that can measure large-volume workpieces with high accuracy but lower than CMM. Nevertheless, they still face challenges with uncertainty, cost, time, and accessibility.

These challenges bring Marker-based Photogrammetry (MbP) into focus. Due to their lower accuracy compared to previous technologies, they are used in applications like measuring raw parts (Mendikute et al., 2017), with comparisons between systems often relying on the VDI/VDE 2634 Part 1 guidelines (Puerto et al., 2022). Despite advantages like ease of use and the lack of a specialized operator, it produces a sparse point cloud and a new issue arises when the environment cannot be adapted, making it impossible to place the markers.

Due to the need for obtaining dense point clouds without the involvement of experienced operators and without a cost increase, there is a clear necessity to explore Markerless Photogrammetry (MP) techniques. Previous research has primarily focused on the achievable accuracy of this technology in contexts like heritage reconstruction (Kingsland, 2020) or drone-based large-scale industrial scene reconstructions (Machado et al., 2021).

Another focus for this technology has been reverse engineering, where it shines thanks to the relatively low cost in comparison to other technologies. One such work is the one presented in (Petruccioli et al., 2022) where two MP software and a 3D reconstruction system for reverse engineering of small parts in a specially prepared scenario are compared, achieving accuracies down to ± 0.3mm.

In (Nikolov and Madsen, 2016), introduced MP software tools and conducted both qualitative and quantitative benchmarking focused on small objects, close-range applications, and large-scale scenarios. Agisoft Metashape[1] stood out for its speed. Similarly, other studies, such as (Enesi and Kuqi, 2023), demonstrated that Agisoft Metashape maintained high accuracy, with errors consistently under 0.1 cm, outperforming software like Meshroom[2] in both speed and accuracy.

The comparison of photogrammetry and laser scanning in (Angheluţă and Rădvan, 2020) highlighted photogrammetry's flexibility with translucent materials. Although laser scanning is faster and more precise, a thorough understanding of each method's limitations was emphasized as essential for optimal decision-making in 3D reconstruction. Recent advancements in 3D scanning for cultural heritage underscore the importance of hybrid methods that combine laser scanning and digital photogrammetry to achieve high-quality models (Kadobayashi et al., 2004).

More recently, (Balloni et al., 2023), conducted a comparative analysis of NeRFs and photogrammetry through a case study involving a statue, employing terrestrial laser scanning acquisition as the reference standard and evaluating cloud-to-mesh distances and roughness values.

This study assesses the feasibility of using MP for measuring large-volume raw parts and its potential industrial applications, considering the accuracy it may achieve. It also considers ma-

[1] https://www.agisoft.com/
[2] https://github.com/alicevision/Meshroom

terial factors, measurement strategies, and the benefits of dense reconstructions.

2. Material and Methods

To address the various advantages and disadvantages of photogrammetry, different types of workpiece models were selected to ensure comprehensive coverage of the technology. Additionally, the aim is to employ the most accurate technologies in terms of measurement to facilitate effective metrological comparisons.

2.1 Models

Three different models, shown in Figure 1, were selected to cover a range of variables such as reflections, textures, machining, surfaces, size, and holes to characterize the accuracy of photogrammetry.

Model Flat (MF): It is a steel reflective object measuring 217x217x15 mm. Its flat, machined specular surface makes it challenging for photogrammetry due to its high reflectivity. The MF was selected to test the system's ability to handle reflective surfaces and small-scale objects.

Model Resin (MR): It is a textured object made of resin, with dimensions of 615x400x396 mm. Its textured, diffuse surface provides ample detail for capturing high-quality 3D scans. The MR model was chosen to maximize the potential of photogrammetry, as it possesses a high degree of texture, making it ideal for capturing detailed surface features.

Model Steel (MS): This is a large, smooth, reflective steel object with dimensions of 1078 x 684 x 510 mm. It features a painted surface, providing minimal texture due to its uniform color, making it a challenge for photogrammetry. Additionally, holes in the model test the system's capability to capture such details accurately.

Figure 1. The three models used in this study, from left to right: Flat, Resin, and Steel.

2.2 Technologies

Given that the **Coordinate Measuring Machine** is a technology designed for measuring sparse points with high accuracy, reaching an accuracy of 4 µm, it is utilized as the ground truth in this work. Specifically, the ZEISS ACCURA model can measure objects up to 2000x3000x1500 mm with this level of accuracy and supports a maximum weight of 5000 kg.

Since sparse measurements are covered with a high level of accuracy, **Laser Tracker** technology is chosen as the ground truth for dense measurements. The Leica Absolute Tracker AT960 is used to measure the SBR semispheres (Hubbs Metrology Solutions SBR-1.500-20MM, mounted on a 1.5-inchdiameter magnetic ball probe seat monument commonly called nests, a Metrologyworks BT-A-Y-BPSM-Y), while the Absolute Scanner AS1 is employed for digitizing parts. This combination enables high-accuracy scanning at speeds of up to 1.2 million points per second. The AS1 achieves an accuracy of ±50 µm at distances up to 30 meters, adhering to the ISO 10360 standard. Similarly, the Leica Absolute Tracker AT960 provides angle accuracy of ±15 µm and distance accuracy of ±0.5 µm/m, also in accordance with ISO standards.

To compare ease of use with accuracy, **Marker-based Photogrammetry** is used, specifically the VSET ©. This photogrammetric system with markers is designed to reduce the time required for best-fit calculation and alignment of large raw parts. VSET© achieves a high accuracy of up to 0.05 mm + 0.02 mm/m and 0.53 mm (k=2) over 12 meters. It uses a Nikon D500 camera with a 22.0 mm focal length, a resolution of 4176 x 2784 pixels, and a shutter speed of 1/200 seconds, with an ISO sensitivity of 500, and operates without a flash

For **Markerless Photogrammetry**, Agisoft Metashape [3] software is selected, a powerful photogrammetry tool used to process digital images into detailed 3D spatial data. The configuration was set with a maximum of 40,000 keypoints and a limit of 10,000 tiepoints. Guided matching was enabled to enhance correspondence accuracy, while stationary points were filtered out to reduce noise. Additionally, MildFiltering was applied to refine the point cloud, and the downscale quality was configured to High for better resolution management.

2.3 Camera configuration:

A Sony Alpha 7III camera equipped with a 35mm lens was utilized for the MP technology.

- **Camera Model:** Sony Alpha 7III
- **Lens:** 35mm sony alpha FE F1.4 ZA
- **Exposure Mode:** Auto
- **Focus:** Auto
- **Flash:** Disabled
- **Image Resolution:** 7952 x 5304 pixels

The Sony Alpha 7III's high resolution was essential for capturing fine details, while the use of auto ISO simulated real-world workshop conditions without introducing artificial lighting. Limited space also made manual focusing impractical, requiring movement around the object to capture multiple angles.

The flash was disabled to avoid reflections or inconsistencies in lighting, ensuring better photogrammetry results. Setting the image resolution to its maximum preserved all object characteristics, enabling more accurate 3D reconstruction in the analysis.

2.4 Data acquisition

Three strategies were designed for data collection to cover all possible points in the photogrammetry process to achieve optimal accuracy, illustrated in Figure 2.

[3] AgiSoft Metashape Professional Version 2.1.0 build 17526 (30 December 2023)

- **Strategy 1:** A standard data acquisition approach to obtain an initial sample. Three different angles, each approximately 45 degrees apart, are used. The entire model is captured in all photos without any cuts or omissions. This strategy is referenced with the set of images taken during the Main pass.
- **Strategy 2:** Provides additional information, enhancing the data set. Five angles, each with a 15º difference, are used, with the camera positioned closer to the model. In this case, the entire model doesn't need to be visible in all photos. This strategy is referenced with the set of images taken during the Main pass and Detail pass 1.
- **Strategy 3:** Focuses on increasing the features of more complex areas that may lack detail in images taken from a greater distance. The objective of this last strategy is to enhance the visibility of subtle features that might not be captured adequately by the previous approaches. This strategy is referenced with the set of images taken during the Main pass and Detail pass 2.

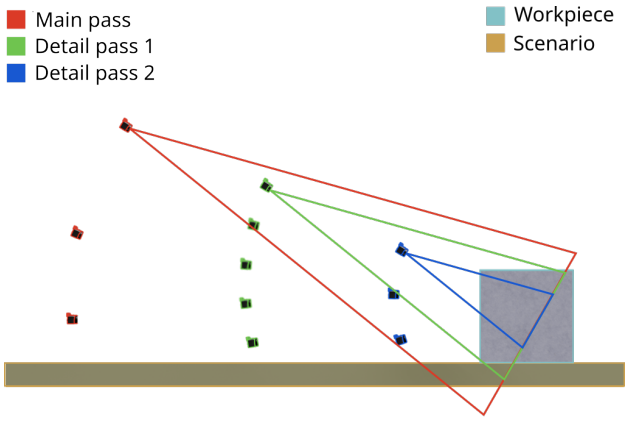

Figure 2. Illustration detailing the three different strategies used.

2.5 Evaluation criteria

To characterize accuracy, the error in the **distance between semispheres**, shown Figure 3 (part a), measured with each technology is calculated. Nests were placed on the models to facilitate the measurement of relative distances between them.

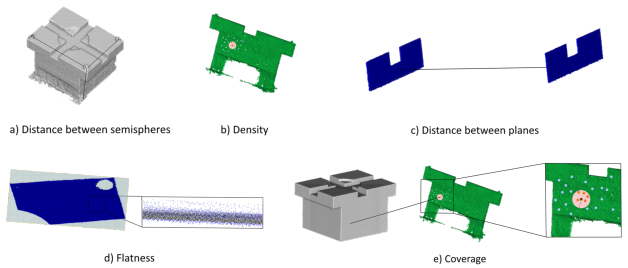

Figure 3. Illustration of the five used comparison criteria.

To analyse the scale change of reconstructions across different technologies relative to the CMM, error measurement symbols for distances between semispheres are retained. The average distance is calculated using absolute values to accurately reflect deviations. Given two points p_1 and p_2 calculate the distance between point 1 to point 2:

$$d_{12} = \sqrt{(x_2 - x_1)^2 + (y_2 - y_1)^2 + (z_2 - z_1)^2} \quad (1)$$

On the other hand, accuracy cannot solely be based on these distances; it must also consider how well the planes have been reconstructed, such as whether they are more inclined than they should be. Therefore, the criterion of **distance between planes**, as shown in Figure 3 (part c), is used, where pairs of planes are identified, and the most extreme points measured with the CMM are calculated, after this rays are drawn from the selected points to calculate the respective distances between the planes. This provides a measure of the deviation in the plane alignment between different technologies.

Furthermore, it is important to consider the accuracy of the reconstructed points relative to the original plane to assess the error in the calculation. For this purpose, the criterion of **flatness**, as shown in Figure 3 (part d), is used, which measures how much the points on the reconstructed surface deviate from the ideal plane.

Given a point cloud $P = \{p_1, p_2, ..., p_n\}$ and a plane $\pi = Ax + By + Cz + D = 0$ for each point p_i calculate de distance to the plane:

$$\text{(a)} \quad \frac{1}{n}\sum_{i=1}^{n} d_i \quad \text{(b)} \quad d_i = \frac{Ax_i + By_i + Cz_i + D}{\sqrt{A^2 + B^2 + C^2}} \quad (2)$$

In addition to accuracy, the quality of the point cloud reconstruction must also be considered, which requires assessing the **density**, as shown in Figure 3 (part b), to determine how many points have been calculated on the plane.

Both volume density, Equation 3 (part a), and surface density, Equation 3 (part b), are measured. Given a point cloud $P = \{p_1, p_2, ..., p_n\}$, for each point p_i calculate volume and surface density, let $N(p_i, r)$ be the number of points within a radius r of p_i.

$$\text{(a)} \quad V_i = \frac{N(p_i, r)}{\frac{4}{3} * \pi * r^3} \quad \text{(b)} \quad S_i = \frac{N(p_i, r)}{\pi * r^2} \quad (3)$$

The density criterion cannot be considered in isolation, as high density may indicate successful reconstruction but could result in inconsistencies if concentrated in one area. Points should be evenly distributed across the plane's surface. Thus, it is crucial to evaluate the criterion of **coverage**, as shown in Figure 3 (part e).

To address how sparse the points are, a uniform point cloud of the model is generated using CAD. For each point in this new cloud, the number of original cloud points within a specified distance was calculated. It is considered covered if more than 5 points are found. Then, the total number of covered points is summed, and the percentage coverage of the plane is calculated.

$$C = \sum_{i=1}^{n} \delta(N(p_i, r) < \tau) \quad (4)$$

Where $\delta(.)$ is the indicator function:

$$f(x) = \begin{cases} \text{if } x \text{ is true} & 1 \\ \text{if } x \text{ is false} & 0 \end{cases} \quad (5)$$

The evaluation criteria used for each model across the measurement technologies are detailed in Table 1. For the flat model, nests were not placed, as doing so would cover more than 50% of the surface, making MP reconstruction impractical, which is the primary focus of this work. Additionally, since the flat model has only one significant plane, the distance between planes was not measured.

		Model Flat	Model Resin	Model Steel
Sparse	Distance between semispheres	-	**CMM** LT MbP	**CMM** LT MbP
	Distance between planes	-	**CMM** LT MbP	**CMM** LT MbP
	Flatness	**CMM** LT	**CMM** LT	**CMM** LT
Dense	Coverage	**LT**	**LT**	**LT**
	Density	**LT**	**LT**	**LT**

Table 1. Representation of evaluation criteria by model and the technology used for measurement. The technology used as the ground truth is highlighted in bold.

3. Results and Discussion

This section provides an overview of the results for each model, detailing the evaluation criteria, measurement technologies, and the three proposed strategies. An industrial case study is also presented, along with data on both acquisition and processing times. Finally, a discussion summarizes the findings across the models and analyzes the effectiveness of each strategy to determine the most suitable approach for the final comparison.

3.1 Model Flat

This model is used to study the results on a reflective object, evaluating the potential of photogrammetry in such cases.

[mm]		LT	MPS1
Mean	P1	1.40e-04	7.24e-04
Std	P1	0.02785	0.0025

Table 2. Results showing the flatness of the model flat. **S:** refers to the different strategies. **P:** refers to the plane of the model.

The flatness results for this model can be seen in Table 2. For P1, the LT scanner shows the lowest mean flatness, indicating greater accuracy in flatness assessment and a closer representation of the ideal geometric plane. In contrast, the MP scanner exhibits more variation in height and curvature. However, the difference between the two methods is minimal, with LT producing smaller deviations from the reference plane for a more precise evaluation in a 3D environment.

[%]	LT	MPS1
P1	100	97.872

Table 3. Results showing coverage % of the model flat. **S:** refers to the different strategies. **P:** refers to the plane of the model.

The results show that coverage is more comprehensive when scanning is done with LT. Nonetheless, the coverage achieved with MP is not far behind, reaching nearly 98% coverage of the part, as shown in Table 3. Reflections can have a greater impact on MP compared to the LT.

		LT	MPS1
Mean volume (pt/mm^3)	P1	23.554	2.047
Std volume (pt/mm^3)	P1	28.388	0.591
Mean surface (pt/mm^2)	P1	62.812	5.459
Std surface (pt/mm^2)	P1	75.703	1.576

Table 4. Results showing the density of the model flat. **S:** refers to the different strategies. **P:** refers to the plane of the model.

Regarding density, there is a clear difference between the LT and MP, as shown in Table 4. First captures many more points through multiple passes over the object, which results in a higher density. However, this also leads to the inclusion of duplicated points, which can be a drawback as it creates very large and cumbersome models.

3.2 Model Resin

This model is used to explore the maximum potential of MP thanks to its texture.

[mm]	LT	MbP	MPS1	MPS2	MPS3
Sph1-Sph2	-0.024	-0.073	0.764	0.228	-1.812
Sph1-Sph3	0.046	0.006	0.393	-0.456	-1.389
Sph1-Sph4	-0.011	-0.045	0.490	-0.313	-1.845
Sph1-Sph5	0.045	-0.055	0.214	-0.386	-1.337
Sph2-Sph3	0.026	-0.068	-0.207	-1.247	-2.22
Sph2-Sph4	0.001	-0.072	-0.122	-0.896	-2.113
Sph2-Sph5	0.007	-0.027	-0.005	-1.051	-3.473
Sph3-Sph4	0.01	0.013	-0.281	-1.558	-2.757
Sph3-Sph5	-0.005	0.029	-0.062	-0.755	-1.003
Sph4-Sph5	0.003	0.013	-0.046	-0.893	-3.388
Mean	0.018	0.040	0.258	0.778	2.134
Std	0.023	0.04	0.339	0.516	0.844

Table 5. Results showing error distances between semispheres compared to CMM ground truth. **S:** refers to the different strategies. **Sph:** refers to semispheres placed on the model resin.

As illustrated in Table 5, incorporating images from additional strategies leads to a decline in accuracy due to autofocus variations in focal distance. This issue is more pronounced in S3, where proximity to the model significantly alters focal length, causing a noticeable degradation in reconstruction accuracy. As a result, the increased focus variation from S3 negatively impacts overall performance.

Consistent with the earlier observations regarding the distance between semispheres, the Table 6 shows that the error increases as additional strategies are introduced. Additionally, depicted Table 7 highlights the differences in angles between the planes used for measuring the distances between them.

[mm]	LT	MbP	MPS1	MPS2	MPS3
P5-P8	-0.0266	0.0931	0.1876	-0.8055	-1.0628
P6-P7	0.0417	-0.0490	-1.1558	-1.1515	-1.081

Table 6. Results showing error distances between planes compared to CMM ground truth. **S:** refers to the different strategies. **P:** refers to planes of the model steel.

[Degrees]	LT	MbP	MPS1	MPS2	MPS3
P5-P8	0.0013	0.0045	0.015	0.080	0.015
P6-P7	0.0011	0.0715	0.444	0.214	0.041

Table 7. Results showing error degrees compared to CMM ground truth. **S:** refers to the different strategies. **P:** refers to planes of the model steel.

In this model, the planes appear more irregular, resulting in higher flatness values than the flat model, as shown in Table

8. The LT remains optimal for flatness assessment, while in MP, adding strategies shows minimal differences, with S1 as the most reliable.

[mm]		LT	MPS1	MPS2	MPS3
Mean	P1	0.0619	0.1481	0.1752	0.1923
	P2	0.0733	0.1459	0.1642	0.1859
	P3	0.0740	0.2194	0.2072	0.2003
	P4	0.0787	0.1478	0.1829	0.1757
	P5	0.1207	0.1356	0.1467	0.2439
	P6	0.1212	0.1924	0.2202	0.2241
	P7	0.1417	0.228	0.2393	0.2411
	P8	0.1048	0.1651	0.1856	0.2271
Std	P1	0.0619	0.1083	0.1247	0.1368
	P2	0.0733	0.1104	0.1159	0.1335
	P3	0.0740	0.1225	0.1151	0.1254
	P4	0.0787	0.0927	0.1227	0.1292
	P5	0.1207	0.096	0.1057	0.1427
	P6	0.1212	0.1288	0.1335	0.1381
	P7	0.1417	0.1374	0.1421	0.1435
	P8	0.1048	0.0996	0.1285	0.1307

Table 8. Results showing the flatness of the model resin. **S:** refers to the different strategies. **P:** refers to planes of the model.

This model, which has many visual features, is reconstructed with higher coverage in some areas compared to the LT, as shown in Table 9. This suggested that MP performs quite well in reconstructing objects with a high level of detail.

[%]	LT	MPS1	MPS2	MPS23
P1	99.5517	97.8959	98.4026	90.3970
P2	96.9515	97.6822	97.9923	88.0521
P3	97.2087	99.9949	100	87.4357
P4	88.0818	97.8900	98.2587	89.5968
P5	82.0219	93.0962	94.7724	67.5307
P6	98.9127	75.3162	76.7140	35.2183
P7	92.1595	71.9337	73.8453	62.0680
P8	91.0796	93.5379	95.9422	60.1418
Mean	92.8811	90.9184	91.9909	72.5550
Std	30.1269	10.9601	10.4646	19.8339

Table 9. Results showing coverage % of the model resin. **S:** refers to the different strategies. **P:** refers to planes of the model.

The strategies demonstrate that increasing the number of images and having reference points closer to the object leads to a higher density of reconstructed points because it can detect features on the object that are undetectable from other distances. Consequently, Strategy 3 yields the best results, although it still does not surpass the performance of the LT, as shown in Table 10.

(pt/mm^3)	LT	MPS1	MPS2	MPS3
P1	3.4766	0.2110	0.9927	2.3269
P2	4.2744	0.2191	0.9571	2.2003
P3	3.4725	0.1336	0.8919	2.029
P4	4.073	0.1922	0.9969	2.5174
P5	3.8733	0.2401	0.9865	2.8442
P6	3.478	0.2880	1.0631	2.8602
P7	3.4159	0.3105	1.0866	2.791
P8	4.5927	0.2339	1.1092	2.8915
Mean	3.8321	0.2285	1.0105	2.5576
Std	0.4453	0.0549	0.072	0.3383

Table 10. Results showing the density of the model resin. **S:** refers to the different strategies. **P:** refers to planes of the model.

3.3 Model Steel

The key difference with this model is its lack of texture, which poses a greater challenge for MP.

[mm]	LT	MbP	MPS1	MPS2	MPS3
Sph1-Sph2	-0.025	-0.073	0.013	-0.534	-1.396
Sph1-Sph3	0.002	0.006	0.202	-0.854	-0.413
Sph1-Sph4	-0.01	-0.045	0.114	-1.013	-3.207
Sph1-Sph5	-0.033	-0.055	0.022	-1.100	-3.695
Sph2-Sph3	-0.006	-0.068	-0.469	-1.549	-0.918
Sph2-Sph4	-0.016	-0.072	-0.274	-1.004	-1.688
Sph2-Sph5	-0.027	-0.027	-0.232	-1.251	-2.418
Sph3-Sph4	0.018	0.013	-0.445	-1.056	-0.49
Sph3-Sph5	-0.002	0.013	-0.427	-1.163	-0.385
Sph4-Sph5	0.004	0.029	-0.115	-0.985	-2.598
Mean	0.014	0.040	0.231	1.051	1.721
Std	0.016	0.040	0.244	0.262	1.207

Table 11. Results showing error distances between semispheres compared to CMM ground truth. **S:** refers to the different strategies. **Sph:** refers to semispheres placed on the model steel.

The accuracy issue arising from using images with varying focus is once again evident as described in Table 11. The error increases significantly when transitioning from MPS1 (0.231) to MPS3 (1.721) when incorporating images with abrupt focus changes. This underscores the detrimental impact of focus inconsistency on measurement accuracy.

[mm]	LT	MbP	MPS1	MPS2	MPS3
P5-P8	0.0295	0.0351	0.1783	2.379	0.0728
P6-P7	0.0111	0.08845	6.1321	-1.1515	0.5916

Table 12. Results showing error distances between planes compared to CMM ground truth. **S:** refers to the different strategies. **P:** refers to planes of the model steel.

Furthermore, the error differences between the planes and the angles between them are presented, as summarized in Table 12 and Table 13, allowing us to evaluate how accurately these planes have been reconstructed compared to CMM measurements.

[Degrees]	LT	MbP	MPS1	MPS2	MPS3
P5-P8	0.0168	0.0273	0.0569	0.4156	0.0812
P6-P7	0.0058	0.0694	0.1372	1.6731	0.4589

Table 13. Results showing error distances between angles compared to CMM ground truth. **S:** refers to the different strategies. **P:** refers to planes of the model steel.

In this case, the average flatness is quite similar, possibly due to the reconstruction not being very accurate, resulting in fewer reconstructed points, as shown in Table 14. Consequently, fewer points could contribute to the errors observed in other models. Nonetheless, the standard deviation is significantly higher for MP compared to the LT.

[mm]		LT	MPS1	MPS2	MPS3
Mean	P1	0.0807	0.0529	0.0153	0.1223
	P2	0.0583	0.0127	0.01136	0.0484
Std	P1	0.1074	0.6483	0.5129	0.6010
	P2	0.1541	0.6096	0.6205	0.5502

Table 14. Results showing the flatness of the model steel. **S:** refers to the different strategies. **P:** refers to planes of the model.

In this model, one of the major disadvantages of MP is evident: flat surfaces where there are insufficient visual features for obtaining a good reconstruction, as reflected in Table 15.

In the case of density, it is noted that a large number of points are present, as described in Table 16; however, when combined

[%]	LT	MPS1	MPS2	MPS3
P1	94.5328	36.2824	55.6709	25.0334
P2	95.3785	66.1322	83.7123	43.9620
Mean	94.9556	51.2074	69.6916	34.4977
Std	0.5979	21.1070	19.8283	13.3845

Table 15. Results showing coverage % of the model steel. **S:** refers to the different strategies. **P:** refers to planes of the model.

		LT	MPS1	MPS2	MPS3
Mean volume	P1	5.197	1.649	5.113	2.447
(pt/mm^3)	P2	13.131	1.703	5.586	2.058
Std volume	P1	4.061	0.526	1.911	0.993
(pt/mm^3)	P2	4.653	0.506	1.981	0.918
Mean surface	P1	13.860	4.397	13.635	6.524
(pt/mm^2)	P2	35.016	4.542	14.896	5.487
Std surface	P1	10.830	1.403	5.095	2.648
(pt/mm^2)	P2	12.409	1.351	5.282	2.449

Table 16. Results showing the density of the model steel. **S:** refers to the different strategies. **P:** refers to planes of the model.

with the coverage data, it becomes evident that these points are clustered in specific areas of the surface.

The coverage analysis shows that the points are not evenly distributed, meaning that although the density is high, it does not reflect a uniform distribution across the entire surface. This uneven distribution underscores the importance of considering both density and coverage metrics for a more accurate assessment of the results.

3.4 Measurement time analytics

Measurement time is a crucial aspect in any industrial process, to the point that is one of the filters in the selection process of the technologies. For this reason, a time comparison between technologies was conducted.

[min]	LT	MbP	MP
Flat	40	17	4
Resin	58	20	7
Steel	85	23	9

Table 17. Acquisition and setup times for the studied technologies.

For the acquisition and setup time cost, illustrated in Table 17, unsurprisingly LT was the most consuming as it includes all the processing to have the raw measurement. In contrast, MbP and MP showed significantly shorter acquisition times, with the Flat model taking just 17 minutes and 4 minutes respectively.

[min]	LT	MbP	MP
Flat	42	19 (166 images)	100 (159 images)
Resin	62	24 (266 images)	368 (286 images)
Steel	91	25 (364 images)	186 (243 images)

Table 18. Analysis of the complete (acquisition and post processing) measurement time Markerless Photogrammetry processing times

For this reason, Table 18 shows the total time from the start of the measurement to obtain the raw measurement. It can be seen that MP is particularly time-intensive for complex models, such as Resin that require denser point clouds and extended processing. Simpler geometries like the Flat model lead to shorter processing times and fewer computational demands. This shows the trade-off between model complexity and processing efficiency, where increased model intricacy demands more significant processing efforts to achieve detailed reconstructions, a critical factor in industrial applications. Summing up, it can be seen that the MbP is the fastest (although sparse) measurement system, followed by the LT, leaving the MP as the slowest of the options altogether.

3.5 Pilot case

To evaluate the actual advantages and limitations of the technologies, an industrial case study was conducted where a part was measured within a single day. In this case, all previously discussed technologies were used to take the measurements, except for the CMM, as the part was too large for that technology.

Model Column (MC): It is a large reflective object made of steel, with dimensions of 3187x1376x1117 mm. Its smooth surface and numerous holes present a challenge for photogrammetry, especially in large-scale structures or scenes. The MC allows us to evaluate the system's performance with large objects and complex geometries.

		Model Flat	Model Resin	Model Steel	Model Column
Sparse	Distance between semispheres	-	**CMM** LT MbP	**CMM** LT MbP	**LT** MbP
	Distance between planes	-	**CMM** LT MbP	**CMM** LT MbP	**LT** MbP
	Flatness	**CMM** LT	**CMM** LT	**CMM** LT	**LT**
Dense	Coverage	**LT**	**LT**	**LT**	**LT**
	Density	**LT**	**LT**	**LT**	**LT**

Table 19. Representation complete of evaluation criteria by model and the technology used for measurement. The technology used as the ground truth is highlighted in bold.

The CMM selected for this study cannot accommodate sizes larger than 2000x3000x1500 mm, as mentioned in subsection 2.2, so the Model Column, which exceeds these dimensions, could not be measured using this technology. Therefore, upon reviewing the Table 1, the complete new table with the updated model and the technologies used to evaluate it can be seen in Table 19. Due to the large size of the model, it was not possible to place scale bars on the ground around it, which disrupted the initial strategy of capturing both the ground and the object simultaneously. Attempting to capture both elements from a distance resulted in the scale bars being undetectable.

[mm]	MbP	MPS1	MPS2	MPS3
Sph1-Sph2	0.312	-0.414	1.726	0.195
Sph1-Sph3	0.381	-0.015	2.67	0.110
Sph1-Sph4	-0.132	-0.405	1.081	-0.434
Sph1-Sph5	0.110	-1.410	-1.794	-1.307
Sph2-Sph3	0.007	0.758	0.765	1.128
Sph2-Sph4	0.175	-0.856	2.138	0.065
Sph2-Sph5	0.213	-1.762	-0.760	-1.352
Sph3-Sph4	0.278	-0.744	2.513	-0.486
Sph3-Sph5	0.276	-1.509	-0.304	-1.598
Sph4-Sph5	-0.024	-1.543	-0.968	-1.669
Mean	0.191	0.942	1.472	0.834
Std	0.1239	0.585	0.810	0.929

Table 20. Results showing error distances between semispheres compared to CMM ground truth. **S:** refers to the different strategies. **Sph:** refers to semispheres placed on the model column.

Consequently, the decision was made to position the scale bars directly on the object itself. Notably, unlike previous models, strategy 3 maintained its performance, as shown in Table 20, even when more images with varying focuses were used.

[mm]	LT	MbP	MPS1	MPS2	MPS3
P1-P2	0	0.04892	0.2103	0.9471	1.5990
P1-P3	0	0.04238	0.2543	1.8853	0.4491

Table 21. Results showing error distances between planes compared to CMM ground truth. **S:** refers to the different strategies. **P:** refers to planes of the model column.

Regarding the distance between the planes, as reflected in Table 21, it is observed that MbP continues to exhibit the lowest error. It should be noted that the LT error is 0 because, in this scenario, because is considered the ground truth. The error distances between angles can be shown in Table 22.

[Degrees]	LT	MbP	MPS1	MPS2	MPS3
P1-P2	0	0.05213	0.3987	0.9234	0.9832
P1-P3	0	0.04567	0.1375	1.0234	0.7829

Table 22. Results showing error distances between angles compared to CMM ground truth. **S:** refers to the different strategies. **P:** refers to planes of the model column.

The flatness remains consistent, as previously discussed in the results of the other models, as shown in Table 23.

[mm]		LT	MPS1	MPS2	MPS3
Mean	P1	0.0009	0.0270	0.0809	0.0199
	P2	0.0067	0.0165	0.0025	0.0071
	P3	0.0279	0.2470	0.4134	0.0568
Std	P1	0.0531	0.5588	0.5043	0.5582
	P2	0.0533	0.5629	0.5137	0.5670
	P3	0.0586	0.6685	0.5810	0.6377

Table 23. Results showing the flatness of the model column. **S:** refers to the different strategies. **P:** refers to planes of the model.

Coverage continues improving with the LT, as noted in Table 24, but excellent results are also achieved with MP.

[%]	LT	MPS1	MPS2	MPS3
P1	100	95.8508	80.1608	93.843
P2	99.149	88.1362	96.1103	91.112
P3	97.831	82.2207	92.9444	86.064
Mean	98.9933	88.7359	89.7385	90.3396
Std	1.0928	6.8348	8.4442	3.9466

Table 24. Results showing coverage % of the model steel. **S:** refers to the different strategies. **P:** refers to planes of the model.

As illustrated in Table 25, the previously mentioned point can again be observed, where the high density of the LT is evident due to repeated passes over the same area.

Regarding acquisition time, LT is the slowest, taking up to 72 minutes to digitize 30% of the model. In contrast, MbP and MP took 30 and 10 minutes for the 100% of the model, respectively. Including post-processing 75, 32 (262 images) and 214 (165 images) minutes were required respectively for the complete process.

3.6 Discussion

As it can be observed in the results, summarized in Table 26, the highest accuracy is achieved with the Strategy 1, despite

		LT	MPS1	MPS2	MPS3
μ volume (pt/mm^3)	P1	59.16	0.559	0.932	0.618
	P2	57.53	0.585	0.973	0.639
	P3	105.62	0.591	0.983	0.638
σ volume (pt/mm^3)	P1	36.43	0.144	0.254	0.167
	P2	45.42	0.125	0.217	0.163
	P3	67.24	0.130	0.228	0.136
μ surface (pt/mm^2)	P1	157.75	14.912	24.849	16.476
	P2	153.42	15.595	25.949	16.929
	P3	281.64	15.76	26.224	17.012
σ surface (pt/mm^2)	P1	97.14	0.384	0.678	0.444
	P2	121.12	0.334	0.579	0.436
	P3	179.31	0.3474	0.607	0.364

Table 25. Results showing the density of the model steel. **S:** refers to the different strategies. **P:** refers to planes of the model.

Strategies 2 and 3 providing higher levels of coverage and density. This demonstrates the effect of variations in camera angles, distances (with the resulting focus change), etc. has in the accuracy of the obtained 3D measurements.

	S1		S2		S3	
DBS	-	0.231	-	1.051	-	1.721
[error, mm]	0.2584	0.9416	0.7783	1.4719	2.1337	0.8344
DBP	-	0.2471	-	8.5050	-	1.3288
[error, mm]	0.4156	0.2323	0.6035	1.4162	1.2655	2.0392
Flatness	0.0278	0.0328	-	0.0133	-	0.0852
[mm]	0.172	0.0968	0.1902	0.1656	0.2113	0.0279
Coverage	97.872	51.2073	-	69.697	-	34.497
[%]	90.918	88.736	91.991	89.738	72.555	90.339
Density	2.047	1.748	-	5.385	-	2.246
[pt/mm^3]	0.228	0.5783	1.011	0.963	2.558	0.6302

Model Flat Mode Steel Model Resin Model Column

Table 26. Results markless photogrammetry with different strategies. DBS: Distance between semispheres, DBP: Distance between planes.

To better illustrate the results, Figure 4 presents the point cloud results obtained from MP using Strategy 1. The figure highlights the accuracy and detail captured in the point cloud.

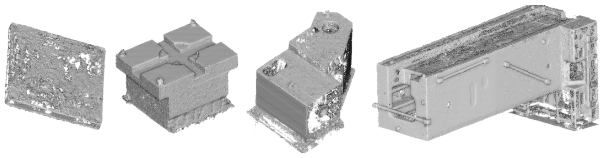

Figure 4. Point cloud results

From an accuracy point of view, as seen in Table 27 the LT demonstrates the highest accuracy among the methods, followed by MbP, with MP using S1 showing the lowest accuracy. However, the latter has shown the capabilities to be used in certain industrial processes where completeness and coverage are as important as ease of use and affordability.

It should be noted that this study was designed to assess the feasibility of the current state of MP for industrial measuring and, while precision is a crucial aspect in evaluating accuracy, due to time constraints, it was not included in this study.

Using LT as the ground truth for dense reconstruction highlights MP's coverage capabilities, which are generally robust across the workpiece, except for certain low-texture areas, such as the steel component, where reconstruction becomes challenging. Photogrammetric measurements tend to have a lower

	LT		MbP		MP	
DBS	-	0.014	-	0.040	-	0.231
[error, mm]	0.0178	0	0.040	0.191	0.258	0.9416
DBP	-	0.0812	-	0.152	-	0.2471
[error, mm]	0.0302	0	0.088	0.091	0.415	0.2323
Flatness	0.00014	0.0807	-	-	0.028	0.0328
[mm]	0.0933	0.0279	-	-	0.172	0.0968
Coverage	100	94.955	-	-	97.872	51.207
[%]	92.881	98.993	-	-	90.918	88.736
Density	23.554	9.131	-	-	2.047	1.748
[pt/mm^3]	3.832	6.438	-	-	0.228	0.5783

Model Flat Mode Steel Model Resin Model Column

Table 27. Results markless photogrammetry with different strategies. DBS: Distance between semispheres, DBP: Distance between planes.

point density compared to LT, potentially because this frequently revisits specific areas, generating a denser, though redundant, dataset that can impact memory use and slow down point-cloud postprocessing. In this context, strategy S3, with a higher number of images, captures finer details that are less visible in S1 and S2, thereby enhancing feature richness. This suggests that S3 could be advantageous when detailed feature visualization is required, even though it may compromise strict measurement accuracy.

Regarding measurement time analytics, the comparative analysis highlights how model complexity impacts performance across technologies. LT shows the longest acquisition times, particularly for complex models like Steel and Column, whereas MbP and MP offer considerably shorter acquisition times. However, processing time in the latter increases notably with model complexity, as seen in the Resin model, where denser point clouds extend processing duration. This underscores the need to balance time efficiency with the level of detail required in each application context.

4. Conclusions

CMM remains the gold standard for accuracy and reliability in dimensional metrology, while the Laser Tracker (LT) with a scanning system provides a robust, accurate measuring system. On the other hand, Markerless Photogrammetry (MP), although less accurate, offers practical advantages for applications requiring sufficient accuracy alongside rapid measurement acquisition times, as well as the ability to generate dense point clouds instead of Marker-based Photogrammetry (MbP).

Among the methods compared, MP demonstrated a high degree of flexibility and ease of use, particularly in terms of capturing dense point clouds at a low cost and with easier deployment. While its accuracy does not match other technologies, the goal of this study was to assess the performance differences to evaluate the potential industrial applicability of this technology. Its margin of error may be acceptable for cases where cost-effectiveness, ease of use, and the inability to alter the environment make it a viable option.

Furthermore, while this technology may not be ideal for high-accuracy tasks, it opens up opportunities in scenarios where adapting the measurement environment or employing highly specialized operators is not feasible. Given these advantages, this method presents a compelling solution for large-scale, lower-accuracy applications that require flexible and cost-effective measurements.

Its most notable flaw, given an application where accuracy provided by the MP may be enough, is its high computational cost and resulting processing times. Looking ahead, future research should focus on refining the process to reduce the time required for processing images, which would enhance its usability in time constrained environments, such as factories. This could potentially bridge the gap between its current limitations in accuracy and the growing demand for efficient, real-time metrology solutions in various sectors.

References

Angheluţă, L., Rădvan, R., 2020. 3D Digitization of translucid materials in cultural heritage objects: a comparative study between laser scanning and photogrammetry. *Romanian Journal of Physics*, 65(7-8), 1–12.

Balloni, E., Gorgoglione, L., Paolanti, M., Mancini, A., Pierdicca, R., 2023. Few shot photogrametry: a comparison between NeRF and MVS-SfM for the documentation of cultural heritage. *The International Archives of the Photogrammetry, Remote Sensing and Spatial Information Sciences*, XLVIII-M-2-2023, 155–162.

Enesi, I., Kuqi, A., 2023. Performance Analysis for 3D Reconstruction Objects in Meshroom and Agisoft—A Comparative Study. *International Journal of Online & Biomedical Engineering*, 19(5).

Kadobayashi, R., Kochi, N., Otani, H., Furukawa, R., 2004. Comparison and evaluation of laser scanning and photogrammetry and their combined use for digital recording of cultural heritage. *International Archives of the Photogrammetry, Remote Sensing and Spatial Information Sciences*, 35(5), 401–406.

Kingsland, K., 2020. Comparative analysis of digital photogrammetry software for cultural heritage. *Digital Applications in Archaeology and Cultural Heritage*, 18, e00157.

Machado, M., Marcellino, G., Salazar, J. D., Regner, D. J., Buschinelli, P., Santos, J. M., Marinho, C., Pinto, T. C., 2021. RPA positioning error influence on close range photogrammetry for industrial instapection. *The International Archives of the Photogrammetry, Remote Sensing and Spatial Information Sciences*.

Mendikute, A., Yagüe-Fabra, J. A., Zatarain, M., Bertelsen, , Leizea, I., 2017. Self-Calibrated In-Process Photogrammetry for Large Raw Part Measurement and Alignment before Machining. *Sensors*, 17(9).

Nikolov, I., Madsen, C., 2016. Benchmarking close-range structure from motion 3d reconstruction software under varying capturing conditions. Springer, 15–26.

Petruccioli, A., Gherardini, F., Leali, F., 2022. Assessment of close-range photogrammetry for the low cost development of 3D models of car bodywork components. *International Journal on Interactive Design and Manufacturing*, 16(2), 703–713.

Puerto, P., Heißelmann, D., Müller, S., Mendikute, A., 2022. Methodology to Evaluate the Performance of Portable Photogrammetry for Large-Volume Metrology. *Metrology*, 2(3).

Savio, E., De Chiffre, L., Schmitt, R., 2007. Metrology of freeform shaped parts. *CIRP annals*, 56(2), 810–835.